Results in Physics 8 (2018) 52–56

Contents lists available at ScienceDirect

Results in Physics

journal homepage: www.journals.elsevier.com/results-in-physics

Bending and splitting of spoof surface acoustic waves through structured rigid surface

Sujun Xie, Shiliang Ouyang, Zhaojian He, Xiaoyun Wang, Ke Deng *, Heping Zhao *

Department of Physics, Jishou University, Jishou 416000, Hunan, China

ARTICLE INFO

Article history:
Received 10 April 2017
Received in revised form 15 November 2017
Accepted 20 November 2017
Available online 26 November 2017

ABSTRACT

In this paper, we demonstrated that a 90°-bended imaging of spoof surface acoustic waves with subwavelength resolution of 0.316λ can be realized by a 45° prism-shaped surface phononic crystal (SPC), which is composed of borehole arrays with square lattice in a rigid plate. Furthermore, by combining two identical prism-shaped phononic crystal to form an interface (to form a line-defect), the excited spoof surface acoustic waves can be split into bended and transmitted parts. The power ratio between the bended and transmitted surface waves can be tuned arbitrarily by adjusting the defect size. This acoustic system is believed to have potential applications in various multifunctional acoustic solutions integrated by different acoustical devices.

Conventional surface acoustic waves (SAWs), e.g., Rayleigh surface waves [1], have been widely applied in electronics, microfluidics, and geophysics. The SAWs essentially arise from the coupling between longitudinal and transverse waves, and thus the dispersion relations mainly depend on the material parameters. Recently, SAWs on various artificial structures, such as phononic crystals [2–7] and corrugated rigid interfaces [8–22], have attracted a great deal of interest. Extraordinary attention has been focused on the case of rigid interface. It is well known that a perfectly rigid smooth surface does not support any SAWs. However, periodically corrugated rigid interfaces have been reported to support a new kind of SAW which originates from the coupling among the acoustic waves localized in the grooves. This kind of new SAW is analogous to the spoof surface plasmon polariton (Spoof SPP) propagating on the periodically structured perfect conductor [23,24], and thus is named as spoof surface acoustic waves (SSAWs). Compared with conventional SAWs, the characteristic of SSAWs can be engineered more flexibly since their dispersion properties are closely related to the geometrical parameters of surface structures rather than the material parameters. Profited from this, many novel applications such as enhanced transmitting [10–13], imaging [15,16], rainbow trapping [17], spatial separating [18], focusing [19] or guiding [20] of SSAWs have been realized in the past few years. For examples, by exciting SSAWs on one-dimensional (1D) textured sound-hard plate, enhanced acoustical transmission and beaming effect have been observed [10–13]. The directional excitation of the SSAWs has also been realized by an epoxy plate patterned with 1D periodical bump plus a pair of asymmetric narrow slits milled through [21]. The acoustic rainbow trapping has been realized through varying linearly 1D periodic groove depth [17,18]. By extending the SSAWs to two-dimensional (2D) textured surface, a subwavelength image with diffraction limit has been obtained both numerically and experimentally [16]. In addition, focusing of SSAWs on a rigid surface engraved with gradient-index array of cylindrical holes has also been observed [19].

In this paper, we proposed an efficient sharp bending scheme for SSAWs by constructing a prism-shaped surface phononic crystal (SPC). Similar to previous studies on acoustic bulk waves in phononic crystals [25–28], profited from the broad flat equi frequency contour (EFC) and total internal reflection (TIR), a 90°-bended imaging with subwavelength resolution of 0.316λ has been achieved. Additionally, a splitting scheme for the SSAWs is proposed by introducing a line-defect into a square surface phononic crystal with interfaces along the ΓM direction. As the combined results of TIR effect and tunneling effect at line-defect, an incoming point source can be split into bended and transmitted source with an arbitrary power ratio by adjusting the interface widths of boreholes. These results are believed to promote the development of SSAWs based OnChip devices in integrated acoustic applications. Here, it is worth to mention that we focus the SSAWs on rigid SPCs, and we do not consider the piezoelectric/piezomagnetic effects. Whereas in recent years there is growing attention focused on piezoelectric/piezomagnetic effects on phononic crystals [29–31]. It will be our next goal to merge the piezoelectric/piezomagnetic effects onto SAWs, which can introduce more physics and more flexibility to tune SAWs.

* Corresponding authors.
E-mail addresses: dengke@jsu.edu.cn (K. Deng), phhpzhao@jsu.edu.cn (H. Zhao).

https://doi.org/10.1016/j.rinp.2017.11.024
2211-3797/

Our system consists of a square lattice of boreholes drilled in a rigid plate. A unit cell of the structure is shown in Fig. 1(a). The width of the borehole is a = 16 mm, the depth of the borehole is h = 40 mm, the thickness of plate is l = 50 mm, and the lattice period is d = 20 mm. The whole structure is placed in air, as schematically shown in Fig. 1(b). The material parameters in our calculations are ρ = 7670 kg/m^3, C_L = 6010 m/s, and C_T = 3230 m/s for steel, ρ = 1.3 kg/m^3 and C_L = 342 m/s for air. Here, ρ represents mass density, C_L represents the velocities of longitudinal waves and C_T represents the velocities of transverse waves. All results in this paper are calculated by the finite-element method (FEM) of the commercial software platform COMSOL Multiphysics.

Fig. 2(a) gives the first band of the SSAWs along the ΓX direction and ΓM direction. It is observed that the first bands are below the air line (gray dashed line). So the SSAWs are nonleaky and can be confined to the surface of SPC. The EFCs of SSAWs are also shown in Fig. 2(b). We can see that the EFC at 1930 Hz displays a flat contour along the ΓM direction. The EFC of bulk acoustic waves in air at 1930 Hz (the magenta dashed circle) is also plotted in Fig. 2(b). It is worth noting that the EFC for SSAWs is obviously broader than that of air. According to the Snell's Law and our previous studies [25,26], most propagating modes and evanescent modes of point source will refract into SPC's eigenmodes, as the eigenmodes of SPC can be excited when corresponding parallel components $k_{//}$ of wave vectors k [k_1, k_2 and k_3 in Fig. 2(c)] in air along the interface direction are equal to parallel components of wave vectors q [q_1, q_2 and q_3 in Fig. 2(c)] in SPC. These refracted acoustic waves propagate in SC along the same directions (ΓM direction) as the group velocity which are perpendicular to SC's EFC, as indicated by the yellow thick arrows in Fig. 2(c). Therefore, if a source is placed in air near the interface, then transmits through the SPC by self-collimation along the ΓM direction, finally images in the export with subwavelength details. In addition, if we cut the SPC along ΓX direction, the parallel components [$q'_{//}$ in Fig. 2(d)] of wave vector q' [q'_1, q'_2 and q'_3 in Fig. 2(d)] along the ΓX or XM direction (the interface of SPC and air) in SPC will fall outside the EFCs of air, then propagating modes [k'_1, k'_2 and k'_3 in Fig. 2(d)] of air cannot be excited. Thus, the excited eigenmodes in SPC will undergo a total internal reflector (TIR) at a SPC-air interface along the ΓX direction. To demonstrate these analyses, we construct a drilled plate with 841 holes [see Fig. 1(b)] and then cut the plate along ΓX direction to form a prism structure [see Fig. 3(a)]. An acoustic point source with frequency of 1930 Hz is placed at the origin of XY coordinates in Fig. 3(a) to excite the self-collimated surface modes of the SPC, which is 6 mm away from the drilled plate. Perfectly matched layers (PML) boundary condition is used in the simulation to absorb the outgoing waves. The numerical result for the pressure field of the system is shown in Fig. 3(a). We can see that the SSAWs are successfully excited by the point source and transmitted as a self-collimated beam, and then bended 90° due to the TIR effect as expected above. After transmitting from the prism SPC, the output SSAWs form a nearfield imaging spot in the exit interface as analyzed in Ref. [22], which is a subwavelength image. In Fig. 3(b), we give the intensity distributions along the y direction parallel to the output interface at the imaging area. The full width at half maximum (FWHM) of the image is about 56 mm or approximately 0.316λ (λ = 177 mm), demonstrating that a subwavelength imaging is achieved through the SSAWs.

We can see from Fig. 3(a) that the acoustic field amplitude decays exponentially into air at the interface when the TIR of self-collimated beams occurs. If such an interface is replaced by a line defect constructed by varying the width of borehole in a row along the ΓX direction, a partial reflection will be expected due to the coupling of the two parts around the defect. In this case, the incoming self-collimated SSAW can be split into two parts at the introduced defect, i.e., a transmitted part along the original propagation direction, and a bended part perpendicular to the original propagation direction. To verify this analysis, we simulated the splitting effect by varying the defect size b in the range of 2 mm to 16 mm (here b = 16 mm means no defect). The calculated pressure field distributions for a point source at frequency 1930 Hz for different b are shown in Fig. 4(a)–(h). It is observed that the incident SSAWs are almost totally reflected by the line defect for b less than 8 mm, behaving as a TIR, as shown in Fig. 4(a)–(d). However, for b greater than 8 mm, transmission efficiency is significantly improved. We can observe from Fig. 4(e)–(h) that, by varying the size of b from 10 mm to 16 mm, the bended power gradually decreases and the transmitted one gradually increases, exhibiting a tunable splitting effect.

As Fig. 4 indicates, the power ratio between bended and transmitted beams is dependent on the coupling efficiency between self-collimated modes and defect modes. To give some more detailed analysis to the mechanism of splitting, we calculated the projected band diagram for SSAWs with a line-defect along the ΓX direction and show the results in Fig. 5(a), in which the defect size b is varying from 2 mm to 14 mm. The band diagrams are calculated by a supercell method. The gray domains in Fig. 5(a) represent the SSAW modes in the system without defect, and the dashed curves with different colors represent dispersion relations of defect modes with different b.

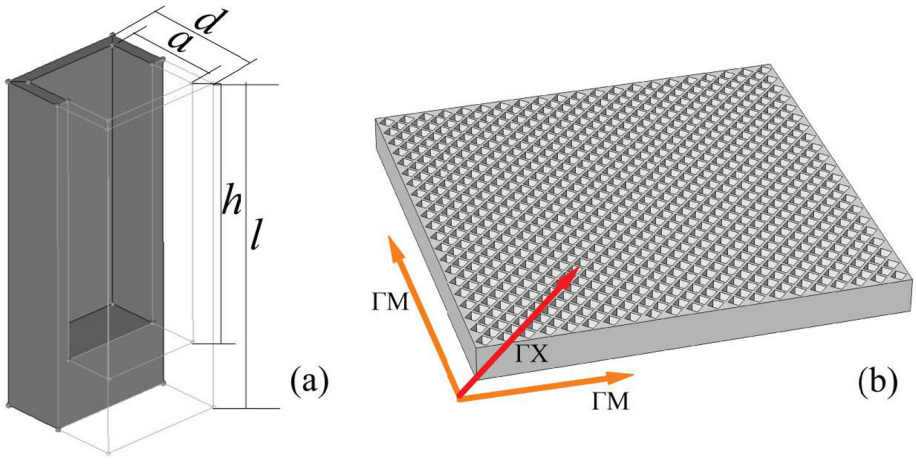

Fig. 1. (a) Schematic illustration of the unit cell of the SPC; (b) Schematic illustration of the SPC cutting along ΓM direction.

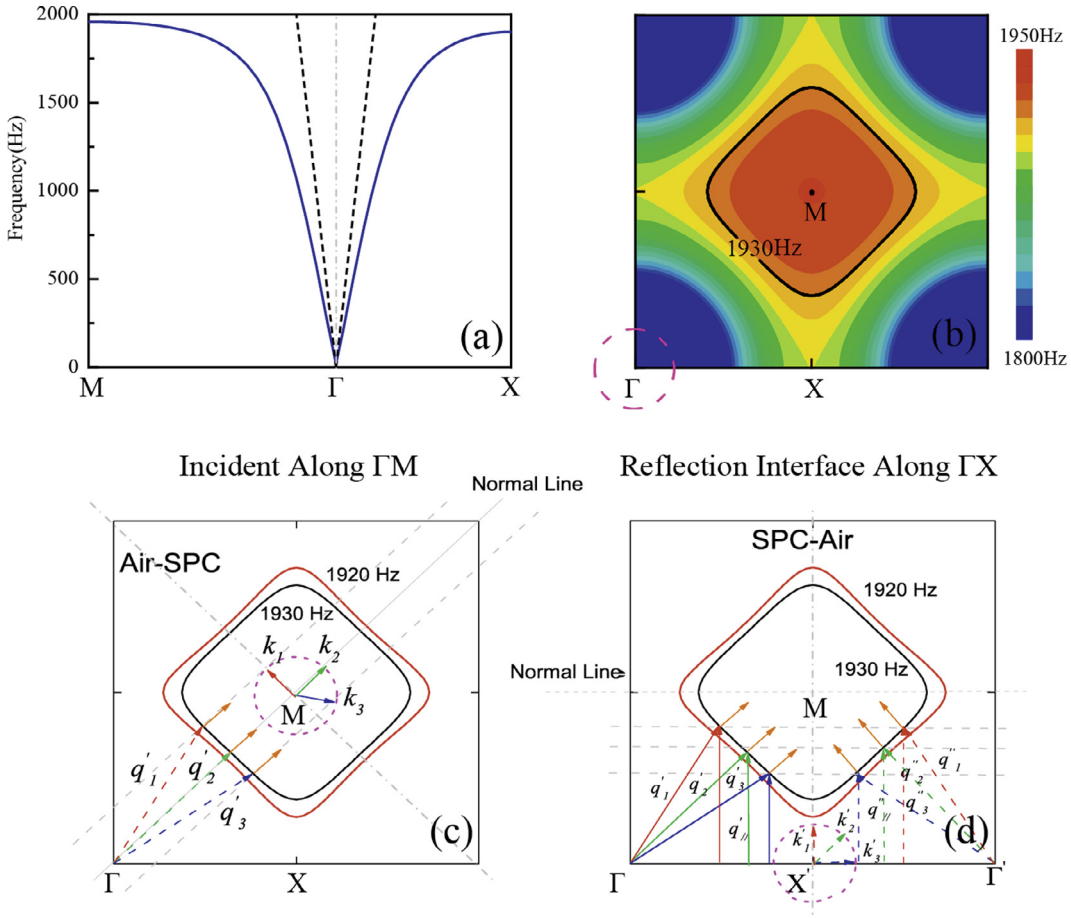

Fig. 2. (a) Dispersion curves (blue solid line) of the SSAWs compared with the air dispersion line (black dashed line); (b) EFC of SSAWs for the SPC. The dashed circle denotes the EFC of air at frequency 1930 Hz. (c) Refraction of three wave vectors from a source into SPC through a ΓM directed interface. (d) Total internal reflection of the collimated modes on the interface of SPC and air along ΓX direction. (For interpretation of the references to color in this figure legend, the reader is referred to the web version of this article.)

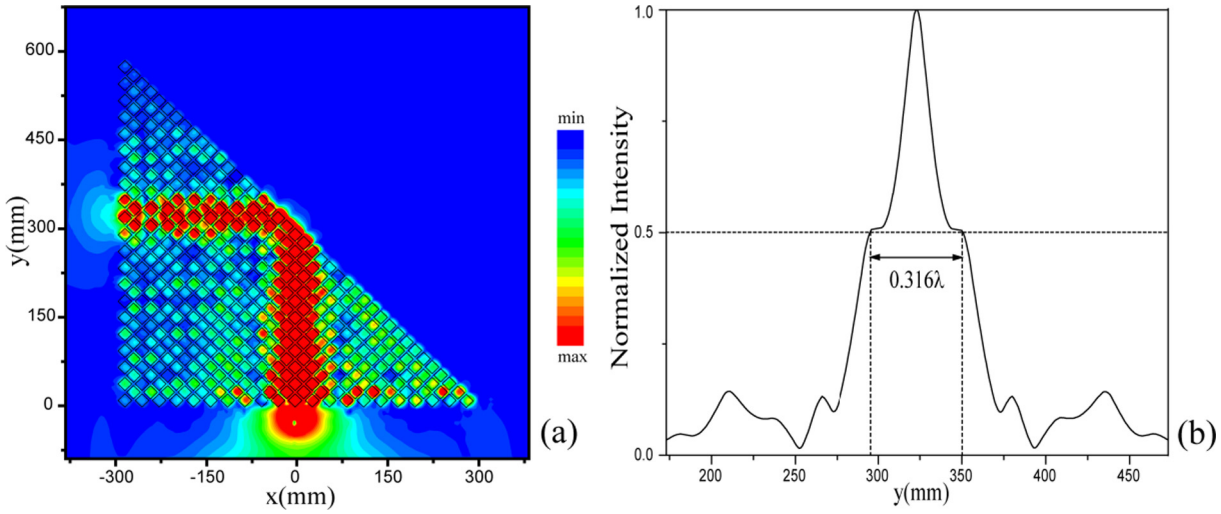

Fig. 3. (a) Pressure field distribution for the bending effect at frequency of 1930 Hz; (b) Normalized acoustic intensity distributions parallel to the output interface at the imaging center.

It can be seen that the frequency of defect modes for defect sizes b from 2 mm to 9 mm is larger than the working frequency 1930 Hz (the black horizontal line), and thus these defect modes can't couple with the self-collimated SSAWs, leading to the weak transmissions as exhibited in Fig. 4. For defect size $b > 9$ mm, the coupling efficiency between self-collimated SSAW modes and defect modes depend on the projection of the k-vector onto the defect direction (here ΓX direction). Strong coupling happens

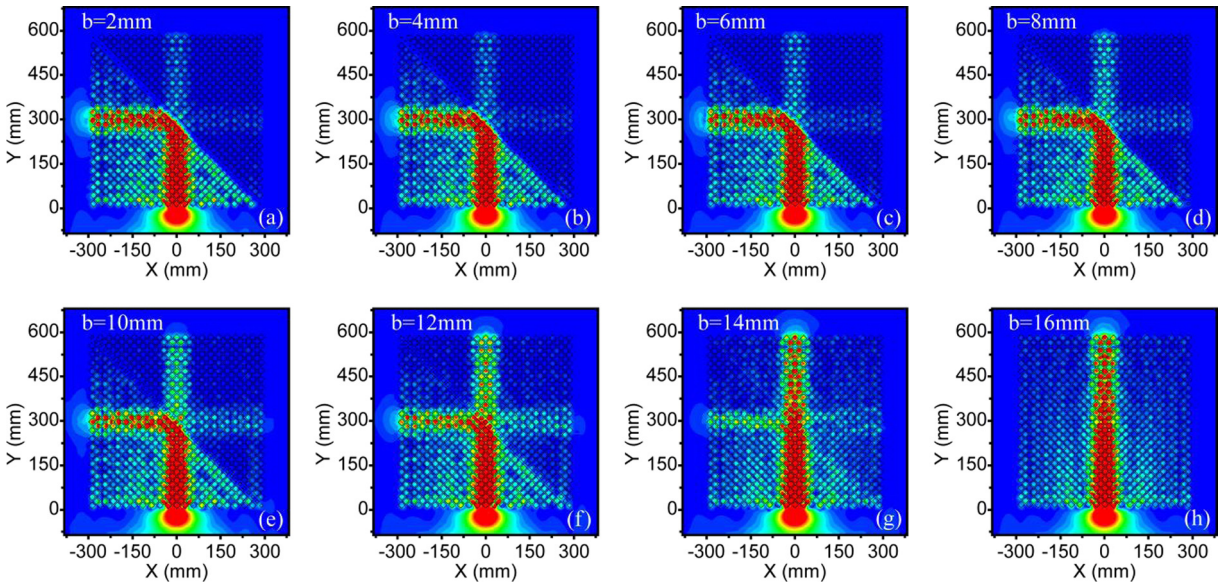

Fig. 4. Splitting effects for different defect size *b* at frequency of 1930 Hz.

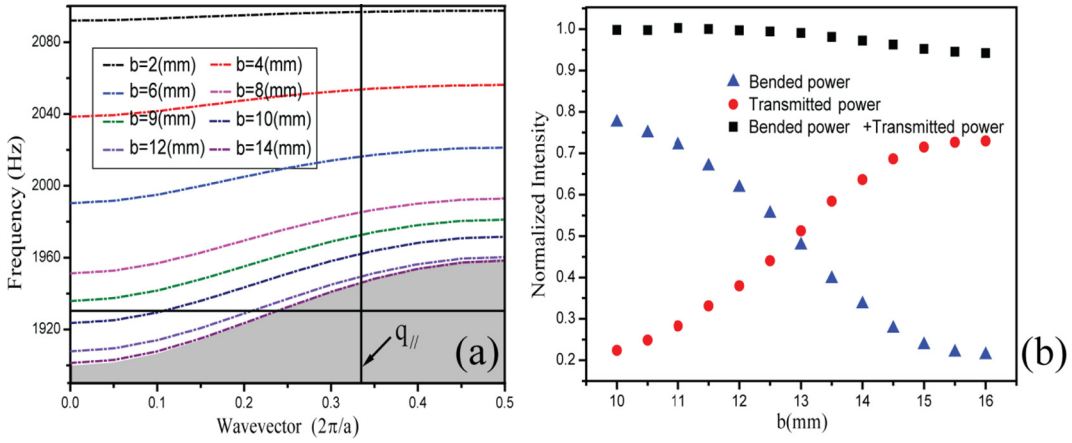

Fig. 5. (a) Band diagrams for the SPC with ΓX direction line defects of different size *b*. The gray domains represent SSAW modes for the system without defect; (b) Bended and transmitted powers for different defect sizes ranging from 10 mm to 16 mm.

when the projection onto ΓX of the reduced k-vector of the self-collimated mode is equal to the reduced k-vector of the defect mode [26]. The projected k-vector of self-collimated mode onto ΓX direction is $q_{//} = 0.335$ at frequency 1930 Hz as show in Fig. 5(a). We can see the reduced k-vector of defect mode is gradually increasing when the defect size increasing from 10 mm to 14 mm. As defect value *b* increases, the reduced k-vector of defect mode is closer to the projected k-vector of self-collimated mode $q_{//}$, which means that the efficiency for the incoming SSAWs coupling to line defect will be increased. To verify this, Fig. 5(b) gives the splitting efficiency at the working frequency (1930 Hz) as a function of *b* with ranging from 10 mm to 16 mm. Here, the bended and transmitted powers were normalized with the sum energy of bended and transmitted SSAWs in the calculation. Fig. 5(b) clearly demonstrates that the incoming self-collimated SSAW beam can be divided into bended and transmitted ones with tunable power ratios by varying *b*. Moreover, the ratio of transmission increases with the increase of defect size *b*, which is in agreement with the coupling theory analysis above.

Conclusion

In summary, we have demonstrated that a 90°-bended imaging of spoof surface acoustic waves with subwavelength resolution of 0.316λ can be realized by a prism-shaped surface phononic crystal, which is composed of borehole arrays with square lattice in a rigid plate. We also demonstrated that by introducing a line-defect into the surface phononic crystal, splitting of spoof surface acoustic waves into a bended part and a transmitted part can also be realized, with the power ratio between the bended and transmitted surface waves being tuned by adjusting the defect size. Such bending and splitting schemes are believed to have potential applications in SSAWs based integrated acoustic solutions.

Acknowledgments

This work is supported by the National Natural Science Foundation of China (Grant Nos. 11464012, 11564012, 11564013, and 11764016), Natural Science Foundation of Hunan province, China

(Grant No. 2016 JJ2100), and Natural Science Foundation of Education Department of Hunan Province, China (Grant No. 16A170). Aid program for Science and Technology Innovative Research Team in Higher Educational Instituions of Hunan Province.

References

[1] Hess P. Phys Today 2002;55:42.
[2] Zhao D, Liu Z, Qiu C, He Z, Cai F, Ke M. Phys Rev B 2007;76:144301.
[3] Assouar MB, Oudich M. Appl Phys Lett 2011;99:123505.
[4] Yudistira D, Pennec Y, Rouhani BD, Dupont S, Laude V. Appl Phys Lett 2012;100:061912.
[5] Oudich M, Assouar MB. J Appl Phys 2012;111:014504.
[6] Addouche M, Al-Lethawe MA, Choujaa A, Khelif A. Appl Phys Lett 2014;105:023501.
[7] Zhao J, Bonello B, Becerra L, Boyko O, Marchal R. Appl Phys Lett 2016;108:221905.
[8] Christensen J, Huidobro P, Martín-Moreno L, García-Vidal F. Appl Phys Lett 2008;93:083502.
[9] Christensen J, Martin-Moreno L, Garcia-Vidal F. Phys Rev Lett 2008;101:014301.
[10] Christensen J, Fernandez-Dominguez AI, Leon-Perez FD, Martín-Moreno L, Garcia-Vidal FJ. Nat phys 2007;3:851.
[11] He Z, Jia H, Qiu C, Peng S, Mei X, Cai F, Peng P, Ke M, Liu Z. Phys Rev Lett 2010;105:074301.
[12] Zhou Y, Lu MH, Feng L, Ni X, Chen YF, Zhu YY, Zhu SN, Ming NB. Phys Rev Lett 2010;104:164301.
[13] Christensen J, Martín-Moreno L, García-Vidal FJ. Phys Rev B 2010;81:174104.
[14] He Z, Jia H, Qiu C, Ye Y, Hao R, Ke M, Liu Z. Phys Rev B 2011;83:132101.
[15] Zhu J, Christensen J, Jung J, Martin-Moreno L, Yin X, Fok L, Zhang X, Garcia-Vidal F. Nat Phys 2011;7:52.
[16] Jia H, Lu M, Wang Q, Bao M, Li X. Appl Phys Lett 2013;103:103505.
[17] Zhu J, Chen Y, Zhu X, Garcia-Vidal FJ, Yin X, Zhang W, Zhang X. Sci Rep 2013;3:1728.
[18] Jia H, Lu MH, Ni X, Bao M, Li XD. J Appl Phys 2014;116:124504.
[19] Ye YT, Ke MZ, Li YX, Wang T, Liu ZY. J Appl Phys 2013;114:154504.
[20] Li C, Ke M, Zhang S, Peng S, Qin C, Liu Z. J Phys D: Appl Phys 2016;49:125304.
[21] Lu JY, Qiu CY, Ke MZ, Liu ZY. Appl Phys Lett 2015;106:201901.
[22] Schwan L, Geslain A, Romero-García V, Groby J. Appl Phys Lett 2017;110:051902.
[23] Pendry JB, Martin-Moreno L, Garcia-Vidal FJ. Science 2004;305:847.
[24] Hibbins AP, Evans BR, Sambles JR. Science 2005;308:670.
[25] Li B, Deng K, Zhao HP. Appl Phys Lett 2011;99:051908.
[26] Li B, Guan JJ, Deng K, Zhao HP. J Appl Phys 2012;112:124514.
[27] Li J, Wu FG, Zhong HL, Yao YW, Zhang X. J Appl Phys 2015;118:144903.
[28] Song Z, Deng K, He Z, Zhao H. Acta Phys Sin 2016;65:094301.
[29] Wang Y, Li F, Huang W, Wang Y. J Mech Phys Solid 2008;56:1578.
[30] Wang Y, Li F, Kishimoto K, Wang Y, Huang W. Eur J Mech A 2010;29:182.
[31] Guo X, Wei P. Ultrasonics 2016;66:72.